Cancer Research

Extracellular Citrate Affects Critical Elements of Cancer Cell Metabolism and Supports Cancer Development *In Vivo*

Maria E. Mycielska[1], Katja Dettmer[2], Petra Rümmele[3], Katharina Schmidt[1], Cornelia Prehn[4], Vladimir M. Milenkovic[5], Wolfgang Jagla[6], Gregor M. Madej[7], Margareta Lantow[1], Moritz Schladt[5], Alexander Cecil[4], Gudrun E. Koehl[1], Elke Eggenhofer[1], Christian J. Wachsmuth[2], Vadivel Ganapathy[8], Hans J. Schlitt[1], Karl Kunzelmann[9], Christine Ziegler[7], Christian H. Wetzel[5], Andreas Gaumann[6], Sven A. Lang[1], Jerzy Adamski[4], Peter J. Oefner[2], and Edward K. Geissler[1]

Abstract

Glycolysis and fatty acid synthesis are highly active in cancer cells through cytosolic citrate metabolism, with intracellular citrate primarily derived from either glucose or glutamine via the tricarboxylic acid cycle. We show here that extracellular citrate is supplied to cancer cells through a plasma membrane-specific variant of the mitochondrial citrate transporter (pmCiC). Metabolomic analysis revealed that citrate uptake broadly affected cancer cell metabolism through citrate-dependent metabolic pathways. Treatment with gluconate specifically blocked pmCiC and decreased tumor growth in murine xenografts of human pancreatic cancer. This treatment altered metabolism within tumors, including fatty acid metabolism. High expression of pmCiC was associated with invasion and advanced tumor stage across many human cancers. These findings support the exploration of extracellular citrate transport as a novel potential target for cancer therapy.

Significance: Uptake of extracellular citrate through pmCiC can be blocked with gluconate to reduce tumor growth and to alter metabolic characteristics of tumor tissue. *Cancer Res; 78(10); 2513–23. ©2018 AACR.*

Downloaded from http://aacrjournals.org/cancerres/article-pdf/78/10/2513/2764970/2513.pdf by guest on 13 September 2024

Introduction

Cancer cells display high metabolic activity to meet their demand for energy and precursors for macromolecular biosynthesis. This includes production of large amounts of fatty acids that serve as essential components of cell membranes and substrates of β-oxidation. Increased mitochondrial β-oxidative activity is associated with some neoplasms like, for example, cervical and breast cancer (1).

Citrate is the primary substrate for fatty acid synthesis and is metabolized in the cytoplasm by ATP-citrate lyase. Citrate contributes to amino acid synthesis, which is critical for proliferating cells. Importantly, however, the origin of citrate in cancer cells is not known. Potential sources of citrate are the Krebs cycle and reductive carboxylation of α-ketoglutarate originating from glutaminolysis (2). In this study, we tested a new hypothesis, where part of the citrate pool is provided externally to cancer cells. Consistent with this hypothesis, decreased blood citrate levels have been associated with some tumors including those in the lung, bladder, and pancreas (3).

Our present study focuses primarily on prostate cells, because citrate levels differ dramatically between healthy and cancerous glands. Therefore, to examine the relationship of citrate to disease, we studied human benign prostate epithelial PNT2-C2 cells that synthesize and release citrate (4) versus malignant prostate PC-3M cells shown previously to import citrate (5). We show that cancer cells take up citrate from the extracellular space under physiological conditions (~200 μmol/L citrate) and have determined the corresponding origin of the plasma membrane citrate transporting protein (pmCiC, variant of the SLC25A1), as well as identified a pmCiC inhibitor. Evidence for metabolism of extracellular-derived citrate is provided, as well as data indicating effects on Krebs cycle activity, glucose metabolism and basic cellular processes. Moreover, we provide evidence that blocking of the pmCiC *in vivo* results in decreased human tumor growth in immunodeficient mice and altered tumor metabolism. Histopathological studies demonstrate pmCiC (variant of the SLC25A1) expression in tumor cells of different human cancers and correlate its abundance with cancer aggressiveness. This study

[1]Department of Surgery, University Hospital Regensburg, Regensburg, Germany. [2]Institute of Functional Genomics, University of Regensburg, Regensburg, Germany. [3]Institute of Pathology, University Hospital Erlangen, Friedrich-Alexander University Erlangen-Nuremberg, Erlangen, Germany. [4]German Research Center for Environmental Health, Institute of Experimental Genetics, Genome Analysis Center, Helmholtz Zentrum München, Neuherberg, Germany. [5]Molecular Neurosciences, Department of Psychiatry and Psychotherapy, University of Regensburg, Regensburg, Germany. [6]Institut für Pathologie Kaufbeuren-Ravensburg, Kaufbeuren, Germany. [7]Department of Biophysics II, University of Regensburg, Regensburg, Germany. [8]Department of Cell Biology and Biochemistry, Texas Tech University Health Sciences Center, Lubbock, Texas. [9]Physiological Institute, University of Regensburg, Regensburg, Germany.

Note: Supplementary data for this article are available at Cancer Research Online (http://cancerres.aacrjournals.org/).

Corresponding Authors: Edward K. Geissler, University Hospital Regensburg, Franz-Josef-Strauss Allee 11, 93042 Regensburg, Germany. Phone: 49-941-944-6961; Fax: 49-941-944-6886; E-mail: edward.geissler@ukr.de; and Maria E. Mycielska, maria.mycielska@ukr.de

doi: 10.1158/0008-5472.CAN-17-2959

©2018 American Association for Cancer Research.

reveals the potential importance of the pmCiC, as well as extracellular citrate availability, on cancer cell metabolism.

Materials and Methods

Cell culture and Western blotting

Cell lines were grown as described previously (5–8). PC-3M cells were received originally from Prof. Chris Foster (University of Liverpool, Liverpool, United Kingdom), PNT2-C2 from Prof. Norman Maitland (Yorkshire Cancer Research, York, United Kingdom), TMK-1 from Dr. Eiichi Tahara (University of Hiroshima, Hiroshima, Japan), L3.6pl from Prof. I.J. Fidler (The University of Texas, M.D. Anderson Cancer Center, Houston, TX), MCF-10A from Prof. Frank Roesl (German Cancer Research Center, Heidelberg, Germany) and BxPC3, HPAF-II, MiaPaCa2 were purchased in 2016 from the ATCC. Although cell lines were not further authenticated, they were grown at low passage numbers from original sources and were kept typically in culture for only 2 months. Cells were tested and confirmed to be mycoplasma free. The following chemicals were used: uniformly ^{13}C-labeled citric acid and glutamine and unlabeled citric acid (Sigma), uniformly ^{13}C-labeled glucose (Cambridge Isotope Laboratories), dialyzed serum (PAN Biotech GmbH) and anti-mCiC (mitochondrial citrate carrier) and pmCiC antibodies (custom-made by GenScript Inc.; ref. 6). Experimental media consisted of RPMI-1640, 5% dialyzed serum, 2 mmol/L glutamine, 25 mmol/L glucose and ± 200 μmol/L citrate, unless otherwise stated. The incubation time varied between 24 and 72 hours, as specified. Mitochondrial protein was extracted using the Mitochondria Isolation Kit (Thermo Fisher Scientific).

Uptake experiments and metabolomics

For stable isotope tracing experiments, cells were washed 3 times with cold PBS before collection. Metabolites were extracted with 80% methanol and measured by HPLC-ESI-MS/MS on an AB SCIEX (Framingham) 4000 QTRAP system. Multiple reaction monitoring (MRM) with one transition each for the unlabeled and the ^{13}C-labeled isotopologues was used. Amino acids were derivatized using propyl chloroformate/propanol as recently described (9) and MRM transitions for the different isotopologues were monitored. Stable isotope tracing data were corrected for natural abundance of ^{13}C using IsoCor (10). Krebs cycle intermediates were separated on a Phenomenex Luna NH2 (150 × 2 mm i.d., 3 μm, Torrence) column with a water (0.1% v/v formic acid)/acetonitrile gradient and ionized in negative mode and MRM detection of selected isotopologues. Lactate and glucose in the media were measured as previously described (11).

Transient siRNA transfections and radiolabeled citrate uptake

^{14}C citrate was purchased from Moravek Biochemicals (Brea, Canada) and experiments were performed as described previously (6). For transient siRNA transfections, cells were preincubated with chloroquine for 2 hours. This was followed by 48 hours incubation with either siRNA (Eurofins Scientific) or mock solution. Western blot analysis or uptake measurements were performed as described elsewhere in the Materials and Methods.

IHC

Human tissue (use granted by the Ethics Commission of the University of Regensburg, number 14-101-0263) was stained with pmCiC (specific antibody), as described before (6).

Patch clamp and homology model

Patch clamp was performed as described before (5). Similar to earlier studies (12) the pmCiC model was generated on the basis of the x-ray structures of ATP/ADP exchanger (pdbIDs: 2C3E, 4C9J and 1OKC) as templates using a standard "automodel" class of MODELLER-9v14 (13). Evaluation was performed using Z-DOPE, a normalized atomic distance-dependent statistical potential based on known protein structures. The finite model was selected on the basis of the assessed scoring functions. Model optimization was performed by applying conjugate gradients, molecular dynamics, and model switch traces to optimize stereochemistry, including non-bonded contacts. However, because no significant improvement was observed, the finite model of the initial modeling procedure was used.

Ligand docking was performed using the flexible-ligand sampling algorithm in AutoDock Vina (14). The input files were generated using AutoDockTools (ADT v1.5.7rc1; ref. 15). Partial charges from the united-atom AMBER force field were used for all receptor atoms (16). Internally calculated atomic affinity grids of the protein were used for the substrate molecule to perform a random walk in the space around the search box. At each step in the annealing, a random displacement is applied to each of the degrees- of-freedom to the center of gravity of the substrate. The displacement results in a new energy, which is evaluated using the grid interpolation procedure against the energy of the preceding step (14). A maximum energy range of 6 kcal/mol was set where binding modes with scores out of this range were discarded. For each docking run the theoretical scoring energy of the respective poses was assessed and the spatial spread was calculated as root-mean-square deviation (rmsd) of atom in one pose with the closest atom of the same element in another pose. This provides a measure for the distance of the respective poses to each other. To compare the respective poses, a quality function was defined [(Em*E0)/rmsd; Em = theoretical scoring energy or a given pose, E0 = highest theoretical scoring energy in all poses of a given ligand, rmsd = rmsd from the pose with the highest theoretical scoring energy].

Flow cytometry (reactive oxygen species)

Studies were performed as before (17). Reactive oxygen species (ROS) production was detected with dihydrorhodamine 123 (Molecular Probes, Darmstadt, Germany). Analysis was performed using a FACSCanto (Becton Dickinson) flow cytometer. At least 10,000 live cells were measured per sample. Dead cells were detected using the Aqua Live/Dead cell kit (Molecular Probes).

Cell growth assay

Cells were plated in 96-well dishes at 500 to 1,000 cells per well. Twenty-four hours after plating in standard culture media, media were replaced with the following solutions: 0.5, 1, or 2 g/L glucose with or without 200 μmol/L citrate; 2 mmol/L glutamine was present in all experimental conditions. Pictures of the cells were taken using the IncuCyte Live-Cell Imaging System (Essen Bioscience). Experiments were conducted for 150 hours and 4 planes of view per well were imaged every 2 hours. Live cell images were collected using a ×10 objective, and cell confluence was calculated using IncuCyte ZOOM 2016 software, which provides real-time cellular confluence data based on segmentation of phase-contrast images.

Downloaded from http://aacrjournals.org/cancerres/article-pdf/78/10/2513/2764970/2513.pdf by guest on 13 September 2024

Targeted metabolomics

Targeted metabolomics measurements of tumor tissue homogenate have been performed in the Genome Analysis Center of the Helmholtz Zentrum München using the Absolute*IDQ* p180 assay (BIOCRATES Life Sciences AG), followed by mass spectrometric analysis. The tissue homogenate was prepared in the following way: to each mg of frozen tumor tissue were added 6 μL of a dry ice cooled mixture of ethanol/phosphate buffer (85/15 v/v). Homogenization was performed using homogenization tubes with ceramic beads (1.4 mm) and a Precellys 24 homogenizer with an integrated cooling unit. For each piece of tumor tissue, 10 μL of homogenate supernatant were applied to the p180 Kit plate. The assay allows the simultaneous quantification of 188 metabolites and includes free carnitine, 39 acylcarnitines, 21 amino acids, 21 biogenic amines, hexoses, 90 glycerophospholipids and 15 sphingolipids. For details see Supplementary Table S1. The measurements with the Absolute*IDQ* p180 Kit and the preparation of tissue samples have been previously described in detail (18, 19). Sample handling was performed with a Hamilton Microlab STAR robotics system (Hamilton Bonaduz AG). Samples were analyzed on an API4000 LC/MS/MS system (Sciex Deutschland GmbH). Data evaluation to quantify the metabolite concentrations was performed with the Met*IDQ* software package, which is an integral component of the Absolute*IDQ* Kit. Concentrations of all metabolites were calculated using internal standards and reported in pmol/mg tissue or the concentrations of tissue homogenate in μmol/L, respectively.

Calcium imaging

The experiments were performed using a ZEISS live cell imaging setup (ZEISS). Fura-2/AM-loaded cells (2 μmol/L, 45 minutes at 37°C) were illuminated with light of 340 or 380 nm (BP 340/30 HE, BP 387/15 HE) using a fast wavelength switching and excitation device (Lambda DG-4, Sutter Instrument). Fluorescence was detected at 510 nm (BP 510/90 HE and FT 409) using an AxioCam MRm CCD camera (ZEISS). ZEN 2012 software (ZEISS) was used to control the hardware and acquire data.

In vivo experiments

Experiments in mice were conducted according to the regulations of the State of Bavaria (permission granted by Regierung von Unterfranken, 55.2-2532.1-34/14). Mice were injected subcutaneously with 500,000 L3.6pl cells. Treatment comprised daily intraperitoneal injections of 10 mg of Na^+ gluconate (Sigma Aldrich, Taufkirchen, Germany) in the treated group starting on day 0. The control group was injected with NaCl only. Tumor volume (width^2 × length × 0.5) and mouse weight were measured every-other day.

Calculations and statistics

Percentage differences denote change of the experimental values as compared with the control data (considered to be 100%). Data are presented as box plots or mean ± SE. Statistical significance was assessed using a two-tailed *t* test, unless otherwise specified. OPLS-DAs were performed for all metabolites R2Y of 0.861 and Q2Y of 0.449 was achieved for all metabolites, whereas a pR2Y of 0.047 and a pQ2 of 0.0155 was found after 2,000 permutations for all metabolites. Calculations were done in R [version 3.2.3; Core Team (2013)], a language and environment for statistical computing (R Foundation for Statistical Computing; URL http://www.R-project.org/ with the package rolls; ref. 20).

Results

To determine whether human cancer and normal cells take up extracellular citrate present at physiological concentrations, we incubated different cell lines with [U-^{13}C]citrate at 200 μmol/L for 24 hours. Citrate uptake was assessed as the intracellular ratio of fully labeled ^{13}C to ^{12}C citrate in prostate (PC-3M), pancreatic (MiaPaCa-2), and gastric (TMK-1) cancer and in non-neoplastic breast (MCF10A) and prostate (PNT2-C2) cell lines. These experiments show that cancer cells take up greater amounts of citrate than normal cells (Fig. 1A). Depending on the conditions, up to one third of the total intracellular citrate pool in cancer cells was derived from uptake of extracellular citrate (Fig. 1B); the strongest effects were observed in cells starved of glucose for 24 hours and in cells grown for 72 hours under hypoxia preceded by 24 hours glucose deprivation, suggesting active regulation of citrate uptake by cancer cells. We conclude that cancer cells take up extracellular citrate present at physiologically relevant levels, and this uptake is influenced by stress conditions.

To exclude the possibility of intracellular Ca^{2+} changes in the presence of extracellular citrate on the observed effects, intracellular Ca^{2+} level was measured using live cell imaging in PC-3M cells loaded with Fura-2 (Supplementary Fig. S1A and S1B). No significant effect of extracellular citrate on intracellular Ca^{2+} levels was detected, excluding citrate chelation of divalent cations as a possible nonspecific action.

Because citrate cannot move freely through cellular membranes, its transport requires a carrier protein. Our previous studies showed that prostate cancer cells have the ability to uptake citrate in a Na^+-dependent manner and that they do not express any of the known plasma membrane di/tri-carboxylate transporters belonging to the SLC13 gene family (5). Electrophysiological characteristics of citrate transport in cancer cells (5) suggested that they could express a transporter similar to the recently cloned K^+-dependent pmCiC (6). Interestingly, Western blotting of PC-3M prostate cancer cells using a specific anti-pmCiC antibody (6) suggested a significant presence of the plasma membrane citrate carrier—pmCiC (Fig. 1C, top). Sequencing of the PCR products confirmed that PC-3M cells expressed unmodified pmCiC (6). pmCiC expression was also found in all the human pancreatic cancer cell lines (MiaPaCa-2, L3.6pl, HPAF-II and BxPC3) studied (Fig. 1C, bottom).

To confirm that the pmCiC is responsible for citrate uptake, we used siRNA to transiently silence pmCiC in PC-3M cells; indeed, a significantly reduced short-term (15 minutes) uptake of ^{14}C-labeled citrate was observed (Fig. 1D). Intracellular content of ^{13}C-citrate was also reduced in the presence of siRNAs in long-term (24 hours) experiments (Supplementary Fig. S1C), confirming the function of pmCiC in extracellular citrate uptake by tumor cells. The pmCiC transporter determined to be expressed in cancer cells and responsible for citrate import has been shown previously to be present in normal prostate epithelial cells, with the function of exporting citrate into the lumen. Interestingly, this transporter has also been found to take up citrate when expressed in HEK cells, suggesting that directional activity of the pmCiC depends on the cell type and plasma membrane composition (6). We conclude that cancer cells express pmCiC in their plasma membrane and this protein is responsible for extracellular citrate uptake.

Downloaded from http://aacrjournals.org/cancerres/article-pdf/78/10/2513/2764970/2513.pdf by guest on 13 September 2024

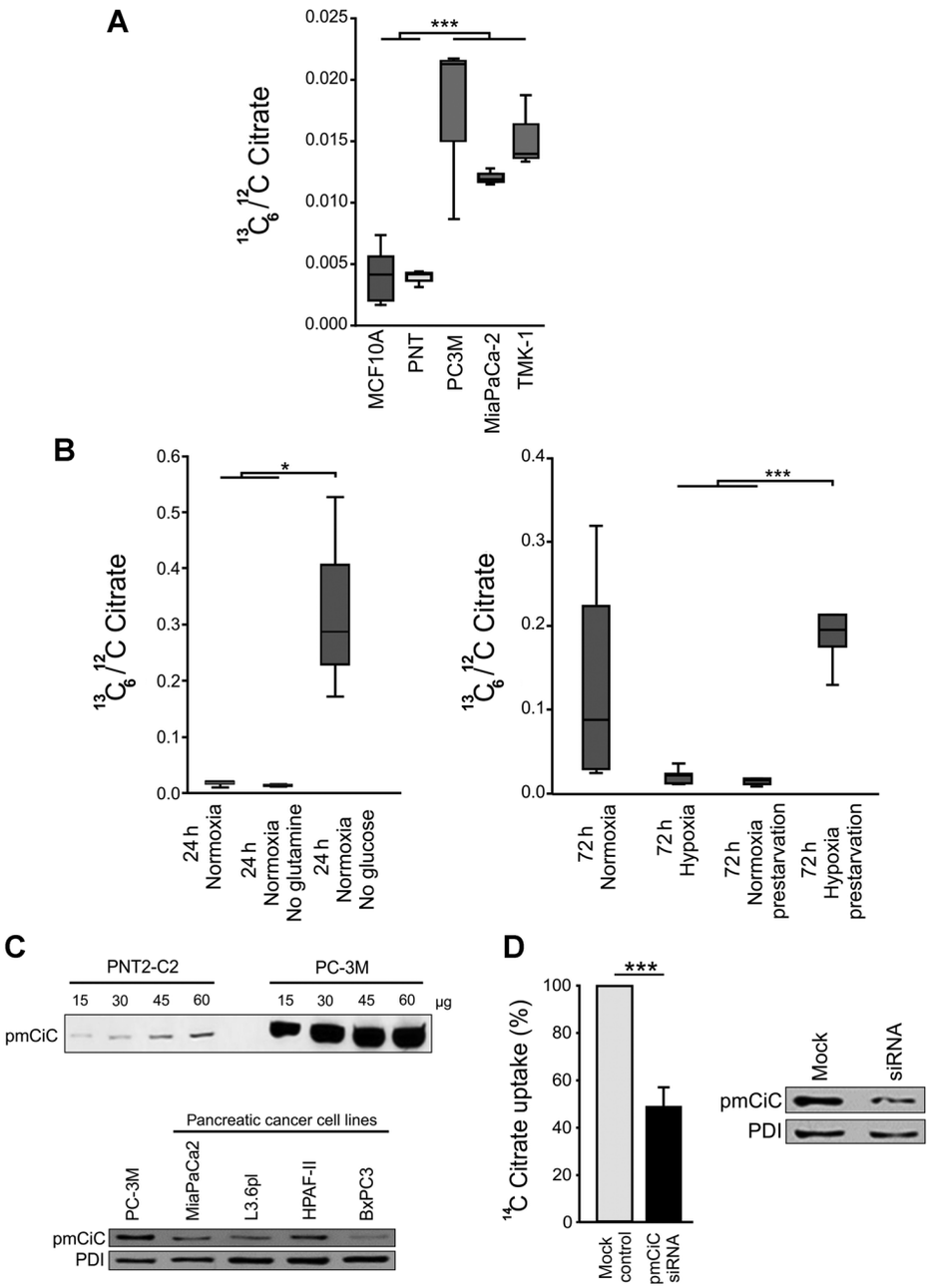

Figure 1.

Cancer cells take up extracellular citrate through the pmCiC. **A,** Intracellular $^{13}C_6/^{12}C$ citrate ratios in normal (MCF10A-breast and PNT2-C2-prostate) and cancer (PC-3M-prostate, MiaPaCa-2-pancreatic, and TMK-1-gastric) cell lines incubated with 200 µmol/L [U-^{13}C]citrate for 24 hours under normoxic conditions in the presence of 10 mmol/L glucose and 2 mmol/L glutamine ($n = 3$, except $n = 6$ for MCF10A). One-way ANOVA across all groups was performed ($P = 0.0003$), followed by a two-tailed *t* test of normal versus cancer cells. ***, $P < 0.001$. **B,** Intracellular $^{13}C_6/^{12}C$ citrate in PC-3M cells grown under different conditions. Glucose deprivation for 24 hours under normoxia and 72 hours glucose deprivation under hypoxia preceded by 24 hours glucose starvation showed significantly higher ^{13}C-citrate uptake into the total intracellular citrate pool. One-way ANOVA with *post-hoc* Tukey-HSD tests for all pairwise comparisons were performed. *, $P < 0.05$; ***, $P < 0.001$; $n = 3$–6. **C,** Expression of pmCiC in total protein derived from PNT2-C2 and PC-3M cells with different protein loadings (top) and PC-3M cells and different human pancreatic cell lines (bottom). Protein disulfide isomerase (PDI) was used as the loading control. **D,** Left, relative to mock-transfected PC-3M cells, ^{14}C citrate uptake is shown for cells with transiently silenced pmCiC. ***, $P < 0.005$; $n = 8$. Right, pmCiC expression levels in PC-3M mock-transfected cells and cells transiently transfected with siRNA specific for the transporter.

To establish the overall effects of extracellular citrate on cancer cell metabolism, changes in the Krebs cycle activity and glycolysis were determined. We compared incorporation of ^{13}C from [U-^{13}C]glucose into intermediates (HPLC-MS/MS) of the Krebs cycle in PC-3M cells in the presence or absence of extracellular citrate. Intracellular metabolite ratios were studied in prostate cancer cells grown under citrate-depleted conditions (dialyzed serum) or with 200 µmol/L citrate-supplemented media (Fig. 2A). Under normoxic conditions, the presence and uptake of extracellular citrate diminished incorporation of labeled carbons from glucose into citrate as reflected in a significantly larger fraction of unlabeled m+0 isotopologue and smaller fractions of labeled isotopologues, albeit reaching significance only in the case of the m+2 isotopologue of citrate (Fig. 2A). Correspondingly, ^{13}C incorporation into fumarate, malate and α-ketoglutarate, was also reduced in the presence of extracellular citrate (Supplementary Fig. S2A). Using flow cytometry, we also determined that ROS levels in PC-3M cells grown with extracellular citrate were decreased by about 20%, compared to cells grown in citrate-depleted dialyzed serum (Fig. 2B, left); use of normal non-dialyzed serum also reduced ROS levels. Extracellular citrate did not significantly affect ROS synthesis in normal PNT2-C2 cells (Fig. 2B, middle). Furthermore, Western blot analysis of the mCiC expression in mitochondria of PC-3M cells showed a significant

Downloaded from http://aacrjournals.org/cancerres/article-pdf/78/10/2513/2764970/2513.pdf by guest on 13 September 2024

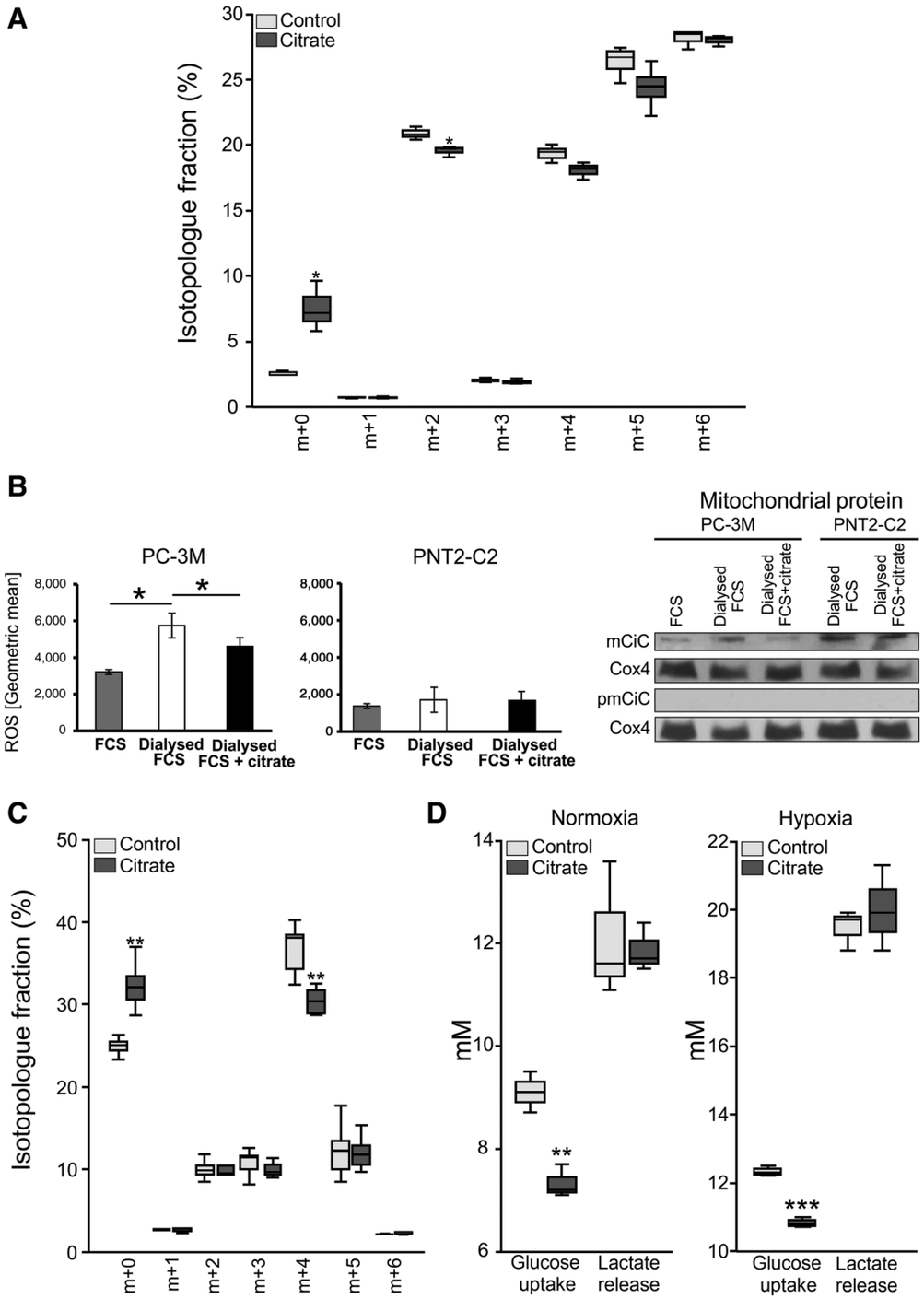

Figure 2.

Extracellular citrate uptake modifies cancer cell metabolism. PC-3M cells were incubated for 24 hours with 4 mmol/L [U-^{13}C]glucose with or without the addition of 200 μmol/L unlabeled citrate. **A,** Isotopologue fractions of citrate are shown. *, $P < 0.05$; $n = 3$. **B,** Differences in ROS synthesis determined by flow cytometry for PC-3M (left) and PNT2-C2 (middle) cells. Cells were incubated in media containing FCS, dialyzed FCS + 200 μmol/L citrate, or dialyzed (citrate depleted) serum only. Shown are geometric means ± SD. *, $P < 0.05$; $n \geq 6$. Right, Western blot analysis of mCiC expression in the mitochondrial fraction of PC-3M and PNT2-C2 cells. Cells were grown in media containing FCS, dialyzed (citrate depleted) serum or dialyzed FCS + 200 μmol/L citrate. As control (3rd row), we used pmCiC-specific antibody to confirm lack of plasma membrane/cytosolic protein presence in mitochondria. **C,** Glutamine metabolism. PC-3M cells were incubated with 2 mmol/L uniformly ^{13}C-labeled glutamine, 25 mmol/L of unlabeled glucose ± 200 μmol/L unlabeled citrate under hypoxic conditions for 24 hours. Isotopologue fractions of citrate are shown. **, $P < 0.01$; $n = 5$. **D,** Amount of glucose consumed and lactate released by PC-3M cells grown for 24 hours with or without 200 μmol/L citrate under normoxic (left) and hypoxic (right) conditions. **, $P < 0.01$; ***, $P < 0.001$; $n = 3$.

Downloaded from http://aacrjournals.org/cancerres/article-pdf/78/10/2513/2764970/2513.pdf by guest on 13 September 2024

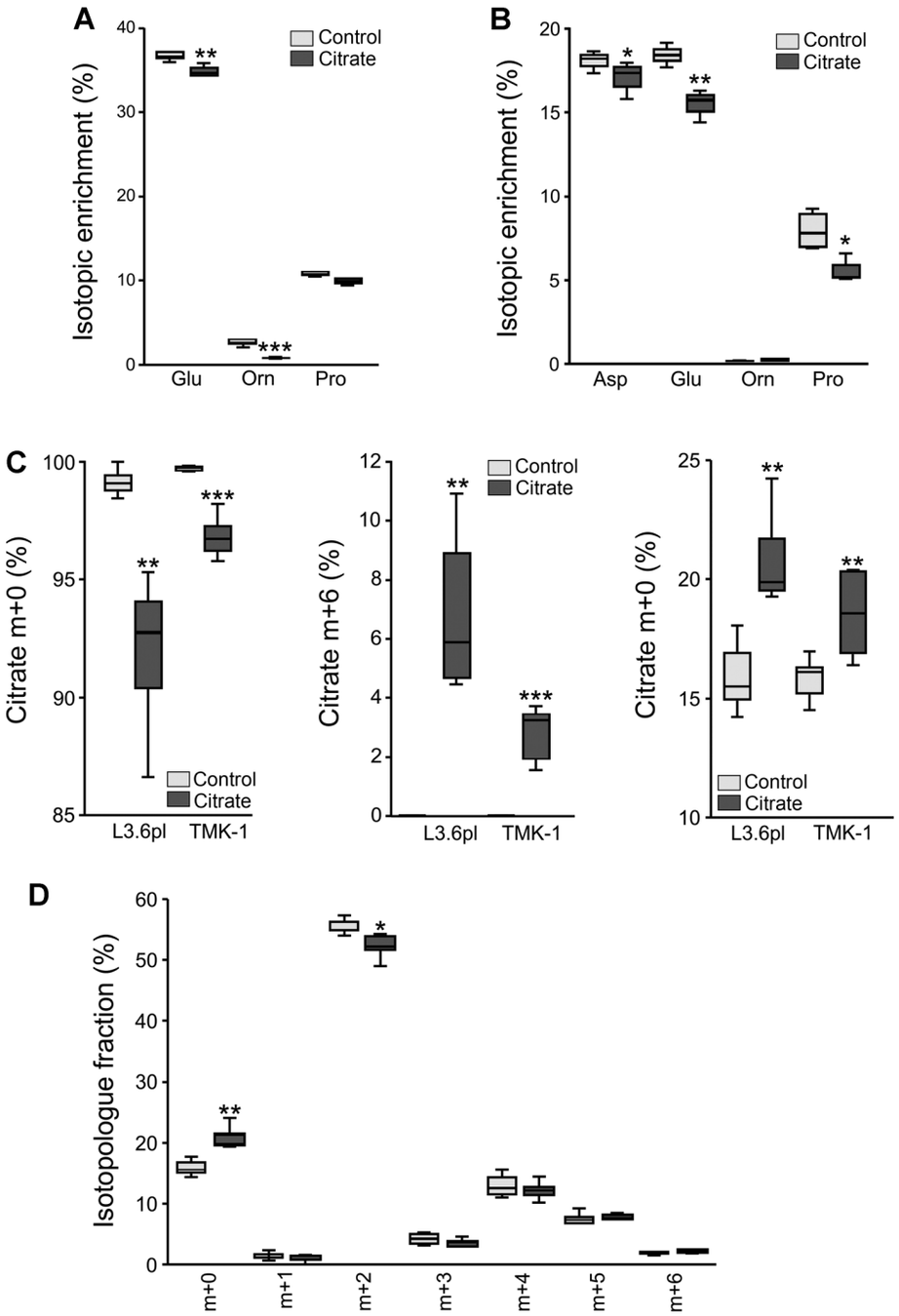

Figure 3.
Extracellular citrate uptake by cancer cell lines of different origin. **A,** Influence of extracellular citrate on the isotope enrichment of free amino acids under normoxic conditions. PC-3M cells were incubated for 72 hours in media supplemented with [U-^{13}C]glucose with or without 200 μmol/L unlabeled citrate. **, $P < 0.01$; ***, $P < 0.001$; $n = 6$. **B,** Influence of extracellular citrate on intracellular amino acid levels. PC-3M cells were incubated under hypoxic conditions for 24 hours in media supplemented with [U-^{13}C]glucose with or without 200 μmol/L unlabeled citrate. Isotopic enrichment in free amino acids is shown. *, $P < 0.05$; **, $P < 0.01$; $n = 4$. **C,** Decrease in unlabeled intracellular citrate (left) and increase in fully labeled intracellular citrate (middle) in human pancreatic (L3.6pl) and gastric (TMK-1) cancer cell lines incubated for 72 hours with or without 200 μmol/L [U-^{13}C]citrate with 25 mmol/L glucose. Right, decrease in unlabeled intracellular citrate in pancreatic and gastric cancer cell lines after 24 hours of incubation with 5.5 mmol/L [U-^{13}C]glucose with or without 200 μmol/L citrate. **, $P < 0.01$; ***, $P < 0.001$; $n = 6$. **D,** L3.6pl cells were incubated for (24 hours) with 5.5 mmol/L [U-^{13}C]glucose with or without the addition of 200 μmol/L unlabeled citrate. Isotopologue fractions of citrate are shown. *, $P < 0.05$; **, $P < 0.01$; $n = 6$.

increase of the mCiC protein in the absence of extracellular citrate, as compared with the conditions with extracellular citrate present (dialyzed serum versus dialyzed serum supplemented with citrate and nondialyzed serum: Fig. 2B, right). This suggests that in the absence of citrate uptake, mitochondria export more citrate into the cytoplasm, which is consistent with no change in the intracellular citrate levels between cells incubated with or without extracellular citrate (Supplementary Fig. S2B). In contrast, no changes in mCiC expression were observed in the case of citrate-producing benign PNT2-C2 cells. Importantly, Western blot analysis confirmed the lack of pmCiC expression in mitochondria (Fig. 2B, right).

Cancer cells take up extracellular glutamine to provide carbon and nitrogen to pathways that support their energy needs and promote cell growth and survival. We examined the influence of extracellular citrate on glutamine metabolism in PC-3M cells under hypoxic conditions by using [U-^{13}C]glutamine (Fig. 2C). The presence of extracellular citrate raised the level of unlabeled citrate in the cells. Moreover, there was a decrease in m+4 citrate, confirming decreased synthesis

Downloaded from http://aacrjournals.org/cancerres/article-pdf/78/10/2513/2764970/2513.pdf by guest on 13 September 2024

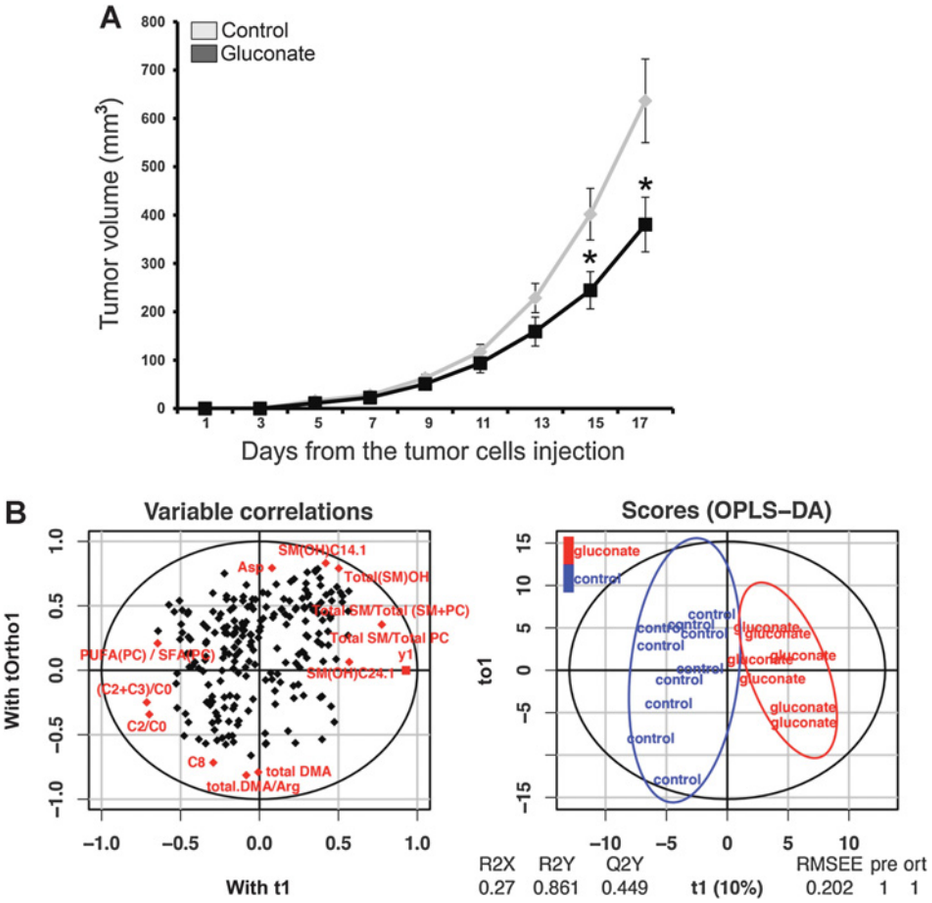

Figure 4.

Gluconate reduces tumor growth and changes metabolic characteristics of cancer tissue. **A,** Mice were injected subcutaneously with human pancreatic L3.6pl cancer cells. Tumor growth was significantly decreased in the group injected daily intraperitoneally with 10 mg of sodium gluconate (in 100 μL); the control group was injected with NaCl (100 μL). **B,** Tumors were removed from the mice and subjected to target metabolite analysis, followed by OPLS-DA analysis. Highest correlations of metabolites to the two groups were calculated to be the ratio of (acetylcarnitine+propionylcarnitine)/free carnitine (abbreviated as C2+C3)/C0, ß-oxidation of even-numbered fatty acids (C2/C0), ratio of poly-unsaturated to saturated glycerophosphocholines [PUFA(PC)/SFA(PC)], hydroxylated ceramide phosphoholine SM(OH)24.1 and SM (OH)C14.1, hydroxylated ceramide phosphocholines [Total(SM)OH], ratio of ceramide phosphocholines (sphingomyelins) to total phospholipid pool [Total SM/Total (SM+PC)], ratio of total ceramide phosphocholines (sphingomyelins) to total glycerophosphocholines (Total SM/Total PC), ratio of total DMA/arginine (Total DMA/Arg) and octanoyl-L-carnitine (C8) and asparagine (Asp). Calculations can be found in Supplementary Fig. S5.

of citrate from glutamine through the forward Krebs cycle. These results confirm that extracellular citrate modifies glutamine usage by cancer cells.

To assess glycolysis, we measured (unlabeled) glucose uptake and lactate release in the media from PC-3M cells incubated with or without 200 μmol/L citrate for 24 hours under normoxic and hypoxic conditions. Interestingly, although lactate production (measured as the absolute amount of lactate per media volume) was unaffected in PC-3M cells incubated with citrate, cells used approximately 22% and 13% less glucose under normoxic and hypoxic conditions, respectively (Fig. 2D).

We further examined the effects of extracellular citrate on the synthesis of intracellular-free amino acids. PC-3M cells were grown in media supplemented with 25 mmol/L [U-^{13}C]glucose ± 200 μmol/L unlabeled citrate. Under conditions of normoxia, in the presence of extracellular citrate, a significant decrease was observed in ^{13}C incorporation from labeled glucose into glutamate (a derivative of α-ketoglutarate) and ornithine (of which glutamate is the precursor), but not proline, which is another glutamate derivative (Fig. 3A). Under hypoxic conditions, there was also decreased ^{13}C incorporation from labeled glucose into glutamate and, in this instance, into aspartate and proline, but not ornithine (Fig. 3B). However, the presence of citrate did not cause a change in absolute levels of amino acids in PC-3M cells (data not shown), which is consistent with a decreased flux of glucose into amino acid synthesis.

To confirm that extracellular citrate uptake and metabolism is not only occurring in prostate cancer cells, we also studied human pancreatic L3.6pl and gastric TMK-1 cancer cells. We observed a significant decrease in the unlabeled citrate level in cells incubated with 200 μmol/L [U-^{13}C]citrate in both cell lines (Fig. 3C, left). As expected, a decrease in the unlabeled citrate was accompanied by a significant increase in fully labeled intracellular citrate levels (Fig. 3C, middle). Moreover, we observed a significant increase in the unlabeled citrate (m+0) in cells incubated with [U-^{13}C]glucose in the presence of unlabeled 200 μmol/L extracellular citrate (Fig. 3C, right). As in the case of the PC-3M cells (Fig. 2A), the presence and uptake of extracellular citrate diminishes incorporation of labeled carbons from glucose into citrate in L3.6pl cells, as reflected in a significantly larger fraction of unlabeled m+0 isotopologue and smaller fractions of labeled isotopologues, albeit reaching significance again only in the case of the m+2 isotopologue of citrate (Fig. 3D). We have also studied the influence of citrate on PC-3M and TMK-1 cell growth under different glucose availability conditions (Supplementary Fig. S3). The effect of citrate was more pronounced in both cell lines when the extracellular glucose level was lower, which is consistent with our results showing that citrate uptake is greater upon glucose starvation (Fig. 1B). Together, these data suggest that citrate is taken up and metabolized by tumor cells of different origin, and therefore may constitute a more general phenomenon.

Downloaded from http://aacrjournals.org/cancerres/article-pdf/78/10/2513/2764970/2513.pdf by guest on 13 September 2024

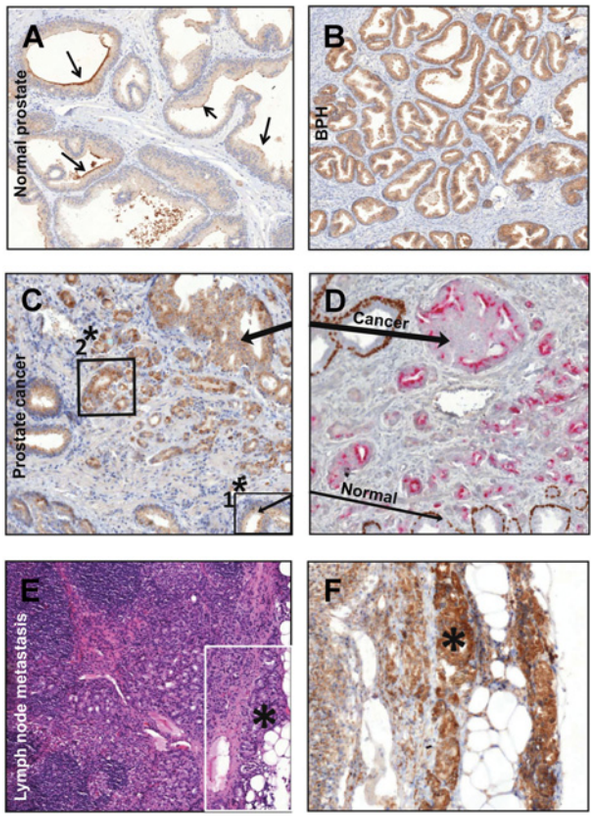

Figure 5.

Cancer cells express pmCiC in primary tumors and at metastatic sites. Tissues in **A, B, C,** and **F** were stained with pmCiC-specific antibody. **A,** Normal prostatic tissue with prominent staining of epithelial cells surrounding the lumen, in particular their apical side (arrows). **B,** Benign prostatic hyperplasia with significant staining of luminal prostate epithelial cells (note stronger staining versus normal tissue; ×70 magnification used for both **A** and **B**). Tissue sections taken from the same cancerous gland stained for pmCiC (**C**) or combined p63 and Racemase/P504S (**D**). Brown staining in **D** indicates p63-positive nuclear and negative Racemase/P504S cytoplasmic staining characteristic for normal cells; cytoplasm-positive Racemase/P504S (pink) and nuclear negative p63 indicate cancer cells. Black arrows show respective areas of tissue to facilitate comparison between pmCiC versus p63-Racemase/P504S staining of cancerous and normal epithelial cells. (**C** and **D,** ×170 magnification). In addition, the areas representative for benign (1*) and cancer cells (2*) from **C** are enlarged and shown in Supplementary Fig. S4. **E** and **F,** Lymph node metastasis of prostatic cells. **E,** ×10 magnification. Lymph node with prostate cancer metastasis stained with hematoxylin and eosin (**E**) and the same tissue stained with pmCiC (**F**). The sequentially sectioned area of the same tissue is indicated with the white frame. Metastatic prostate cancer cells show increased expression of pmCiC (**F,** ×150 magnification). Black stars on both photos indicate the same area of the lymph node.

Because pmCiC and mCiC are encoded by genes located at the same loci, stable silencing of the pmCiC might also affect the mCiC. Therefore, we opted to search for a low-molecular weight inhibitor to test the importance of citrate uptake *in vivo*. We started the search for an inhibitor by exploring the docking behavior of various carboxylic acids, which were randomly selected from the ZINK database (Supplementary Fig. S4A), to a homology model of pmCiC. The majority of observed docking poses clustered at the apex of the central cavity typical for transporters in this family (Supplementary Fig. S4B). Compared with average random carboxylic acids, docking poses of citrate and gluconate displayed higher quality calculated as a quotient of the spatial spread and theoretical scoring energy for binding (Supplementary Fig. S4C). Patch clamp recording on the PC-3M cells confirmed gluconate to be an inhibitor of citrate import through the pmCiC (Supplementary Fig. S4D and S4E). Application of gluconate resulted in a decrease of citrate-induced currents. This effect was irreversible and became larger with every subsequent gluconate application (Supplementary Fig. S4D and S4E).

We then tested the effects of inhibiting citrate uptake with gluconate on tumor growth and metabolism *in vivo*. Application of Na^+ gluconate (given intraperitoneally) decreased subcutaneous human pancreatic (L3.6pl) tumor volume in immunodeficient mice (Fig. 4A). Metabolomic analysis of the tumor tissues from the control and gluconate-treated groups revealed a significantly different metabolic profile (Fig. 4B; Supplementary Fig. S5A–S5D). OPLS-DA analysis of all metabolites identified changes in overall ß-oxidation of fatty acids [indicated by the ratio of acetylcarnitine+propionylcarnitine/free carnitine and ß-oxidation of even-numbered fatty acids (ratio of acetylcarnitine/free carnitine)], activity of fatty acid desaturases (ratio of poly-unsaturated to saturated glycerophosphocholines) and ceramide levels [hydroxylated ceramide phosphoholine SM(OH)24.1 and SM (OH)C14.1, hydroxylated ceramide phosphocholines, the ratio of ceramide phosphocholines (sphingomyelins) to total phospholipid pool, and ratio of total ceramide phosphocholines to

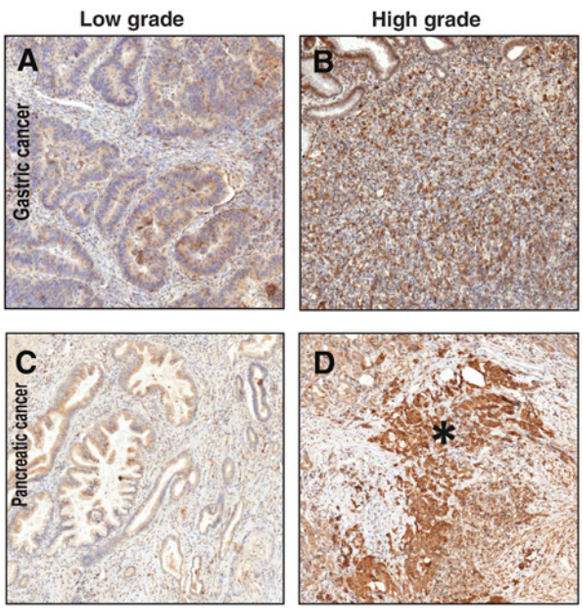

Figure 6.

pmCiC is expressed in cancerous tissues of different origin. **A–B,** gastric cancer. Gastric adenocarcinoma, intestinal (glandular) type with irregular tubular structures is shown in **A**. pmCiC staining in this subtype is weak, focal, and patchy (predominantly apical), as compared with the gastric adenocarcinoma, diffuse type (**B**), with almost all signet-ring cells strongly stained with pmCiC. **C–D,** pancreatic cancer. Moderately differentiated pancreatic ductal adenocarcinoma cells (**C**) stain heterogeneously and weakly positive in the cytoplasm, whereas poorly differentiated pancreatic ductal adenocarcinomas (**D**; *) are strongly positive in a diffuse pattern. **A–D,** ×100 magnification.

Downloaded from http://aacrjournals.org/cancerres/article-pdf/78/10/2513/2764970/2513.pdf by guest on 13 September 2024

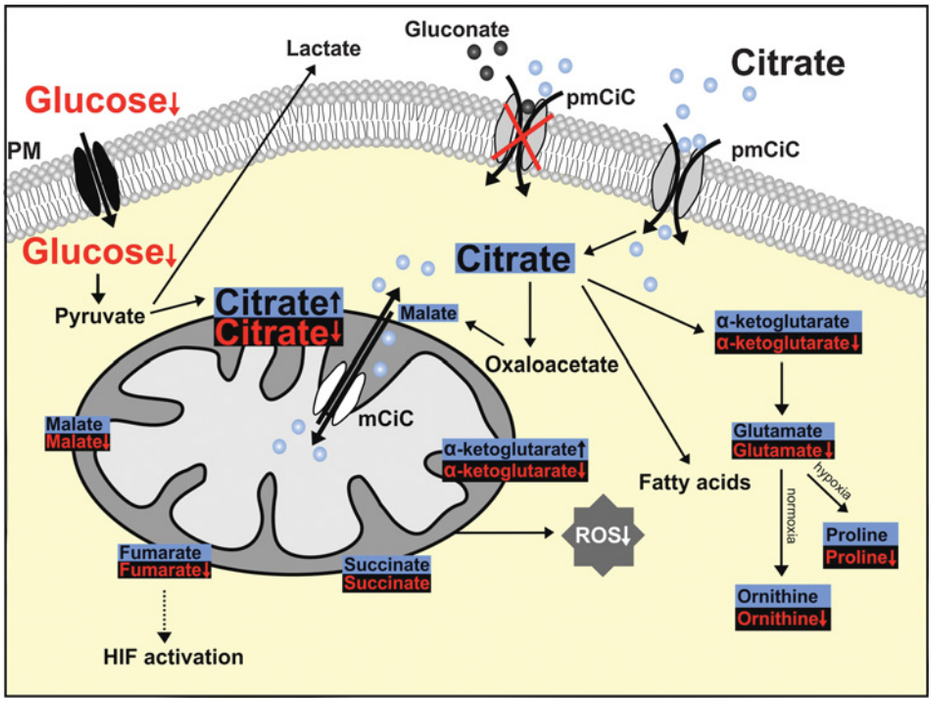

Figure 7.

Scheme of metabolic pathways that interact with extracellular citrate based on the present research and previously published data. Red, labeled substrates derived from ^{13}C glucose; black, unlabeled intermediates derived from unlabeled citrate. Decrease or increase in the labeled carbon incorporation shown with arrows illustrate the changes determined in cells incubated with 200 μmol/L extracellular citrate compared with control conditions (without extracellular citrate). Unlabeled citrate (blue) is taken up by cancer cells through pmCiC and enters primarily cytosolic pathways. Our results indicate that this in-turn reduces mitochondrial citrate export into the cytoplasm and decreases ROS synthesis. Unlabeled extracellular citrate is used partially for glutamate and glutamate-derivative as well as fatty acids synthesis. This accompanied by lower glucose is uptake. Application of gluconate (gray) blocks extracellular influx through pmCiC. Elements in the diagram based on results published by other groups are shown with dotted lines.

total glycerophosphocholines]. Importantly, all these substrates and enzymatic processes are linked to fatty acids (for which citrate is the primary substrate) and fatty acid-derived products that are vital for cancer progression (21, 22). Other metabolite changes concerned activity of protein arginine methyltransferases (ratio of total DMA/arginine) implicated in gene transcription, DNA repair and mRNA splicing (23), and levels of octanoyl-L-carnitine and asparagine, which are known to play a major role in cancer by maintaining amino acid homeostasis, anabolic metabolism and proliferation (24). Altogether, metabolic alterations occurring *in vivo* support our *in vitro* observations that gluconate blocks citrate influx and, consequently, changes citrate supply/metabolism to cancer cells.

To further show relevance of the present findings to human cancer, expression of pmCiC in various human tissues was evaluated by immunohistochemistry. Relevant to our *in vitro* studies using prostate cells, we studied expression of the pmCiC in healthy human and cancerous prostate tissues at different pathological stages from healthy tissue, to benign prostatic hyperplasia, and finally to cancer. According to our experimental findings, we anticipated that the pattern and intensity of pmCiC expression in the prostate might change in the transition to cancer (Fig. 5A–F). Immunohistochemistry for pmCiC showed that healthy prostatic epithelium stained predominantly at the apical part of the cells (Fig. 5A), which is expected as these cells export citrate via the pmCiC. In BPH (benign prostatic hyperplasia), pmCiC staining intensity in epithelial cells was increased, correlating with elevated extracellular citrate levels associated with benign prostatic overgrowth (Fig. 5B; ref. 25). Importantly, diffuse and strong staining of pmCiC was observed in prostatic cancer cells (Fig. 5C) and correlated well with p63/Racemase/P504S cocktail staining (double-staining method, Fig. 5D; ref. 26). Normal prostatic epithelium with characteristic nuclear p63 positivity (shown in Fig. 5D; ref. 26) stained weakly with pmCiC (Fig. 5C-1*; Supplementary. Fig. S6-1*). In contrast, prostatic adenocarcinoma staining with pmCiC was stronger and more evenly dispersed (Fig. 5C-2*; Supplementary Fig. S6-2*), correlating with cytoplasmic Racemase/P504S positivity (Fig. 5D). Immunohistochemical staining of pmCiC was also positive in other malignant tissues including gastric and pancreatic (Fig. 6A–D), breast, glioblastoma, colon and bladder cancer (Supplementary Fig. S7A–S7D). Cancer cells also retained high expression levels of pmCiC at lymph node and bone metastasis sites (Fig. 5E and F; Supplementary. Fig. S7E and S7F). Data obtained in this study also suggest a correlation between the intensity of pmCiC staining and tumor grade (Fig. 6A–D), consistent with the hypothesis that pmCiC expression correlates with cancer development.

Discussion

Our study shows for the first time that extracellular citrate is taken up by cancer cells through the pmCiC and donates carbon to

Downloaded from http://aacrjournals.org/cancerres/article-pdf/78/10/2513/2764970/2513.pdf by guest on 13 September 2024

cancer metabolism (as summarized in Fig. 7). Moreover, blocking of citrate transport with gluconate *in vivo* decreases tumor growth and changes the metabolic characteristics of tumor tissue. pmCiC expression was found in the human cancer types studied indicating extracellular citrate uptake is a common cancer feature. This plasma membrane transporter and the process of extracellular citrate uptake should be recognized in the search for potential novel targets in cancer therapy.

More specifically, we have shown that cancer cells of different origin have the ability to take up extracellular citrate at the level available in blood. Our data show that cancer cells are flexible in their choice of extracellular carbon donors. Switching to an extracellular citrate supply in particular under hypoxic and low glucose conditions appears to facilitate tumor progression, as demonstrated here, for example, for cancer cell proliferation. Interestingly, consistent with our finding, a recent report indicates that senescent fibroblasts release citrate, which could be an additional source of this metabolite for cancer cells *in vivo* (27). Uptake of extracellular citrate also appears critical for lipid biosynthesis and metabolism, as evidenced by metabolite profiling of tumor tissues in our mouse model upon inhibition of citrate uptake by gluconate. A relationship of cancer cells to citrate utilization is supported by our data showing that different human cancer tissues express high levels of the pmCiC especially in advanced tumors and metastases.

We also show in this report that pmCiC responsible for citrate uptake in cancer cells performs this function in a Na^+-dependent manner (5). This finding reveals a significant difference compared to normal prostate epithelial cells that are known to excrete citrate through the pmCiC in a K^+-depending manner (6). Although this important aspect of our study requires further research, the bidirectional mode of citrate transport associated with the pmCiC suggests that posttranslational modifications of the transporter protein, multimer formation and/or altered insertion into the plasma membrane occurs in cancer, versus normal, cells. These structural changes in cancer cells expose the pmCiC as a novel specific target in cancer therapy.

Regarding targeted cancer therapy, we have discovered that gluconate is a specific inhibitor of the pmCiC and its application *in vivo* reduces human pancreatic tumor growth and changes the metabolic characteristics of tumor tissue in mice. Gluconate is considered by the FDA to be a harmless substance and is used in medicine as a heavy metals carrier. Interestingly, disulfiram in combination with Zn^{2+} supplied in the form of zinc gluconate has been used successfully to treat a case of metastatic ocular melanoma in a human (28), but further clinical studies using disulfiram alone (without gluconate) did not show an anti-cancer effect (29). Our research therefore raises the possibility that gluconate contributed to the success of this treatment regime and opens the possibility of pmCiC targeting to testing in cancer patients.

Disclosure of Potential Conflicts of Interest

M.E. Mycielska has ownership interest (including patents) in the plasma membrane citrate transporter for use in the diagnosis and treatment of cancer; patent application no. EP15767532.3 and US15/514,255 (status patent pending). E.K. Geissler reports receiving a commercial research grant from Trizell GmbH, has received speakers bureau honoraria from Novartis, and has ownership interest (including patents); patent pending EP15767532.3 and US15/514,255. No potential conflicts of interest were disclosed by the other authors.

Authors' Contributions

Conception and design: M.E. Mycielska, P. Rümmele, K. Schmidt, H.J. Schlitt, K. Kunzelmann, P.J. Oefner, E.K. Geissler

Development of methodology: M.E. Mycielska, P. Rümmele, M. Lantow, K. Kunzelmann, A. Gaumann

Acquisition of data (provided animals, acquired and managed patients, provided facilities, etc.): K. Dettmer, P. Rümmele, K. Schmidt, C. Prehn, V.M. Milenkovic, W. Jagla, M. Lantow, M. Schladt, G.E. Koehl, E. Eggenhofer, C.J. Wachsmuth, C.H. Wetzel, A. Gaumann, J. Adamski, E.K. Geissler

Analysis and interpretation of data (e.g., statistical analysis, biostatistics, computational analysis): M.E. Mycielska, P. Rümmele, K. Schmidt, V.M. Milenkovic, G.M. Madej, M. Lantow, A. Cecil, C.J. Wachsmuth, K. Kunzelmann, C. Ziegler, C.H. Wetzel, A. Gaumann, J. Adamski, P.J. Oefner, E.K. Geissler

Writing, review, and/or revision of the manuscript: M.E. Mycielska, P. Rümmele, C. Prehn, M. Lantow, A. Cecil, V. Ganapathy, H.J. Schlitt, A. Gaumann, S.A. Lang, J. Adamski, P.J. Oefner, E.K. Geissler

Administrative, technical, or material support (i.e., reporting or organizing data, constructing databases): P. Rümmele, W. Jagla, E.K. Geissler

Study supervision: H.J. Schlitt, E.K. Geissler

Acknowledgments

This study was supported in part by KFO262, German Federal Ministry of Education and Research (BMBF) to the German Center Diabetes Research (DZD e.V.) grant (to J. Adamski) and a fellowship from Bavarian Government to Women in Research and Education (to M.E. Mycielska). We are grateful to Prof. Dr. Philipp Beckhove and Dr. Till Michels (Regensburg Center for Interventional Immunology) for their help with cell proliferation assay. We are grateful to Silke Becker (Helmholtz Zentrum München), Rudolf Jung (Institute of Pathology, Erlangen), Monika Kerscher (Institute of Pathology, Regensburg, Germany), Nadine Nürnberger (Institute of Functional Genomic, Regensburg, Germany), Lydia Schneider and Christine Wagner (Department of Surgery, Regensburg, Germany) for their excellent technical help.

The costs of publication of this article were defrayed in part by the payment of page charges. This article must therefore be hereby marked *advertisement* in accordance with 18 U.S.C. Section 1734 solely to indicate this fact.

Received September 26, 2017; revised February 7, 2018; accepted March 1, 2018; published first March 6, 2018.

References

1. Rodríguez-Enríquez S, Hernández-Esquivel L, Marín-Hernández A, El Hafidi M, Gallardo-Pérez JC, Hernández-Reséndiz I, et al. Mitochondrial free fatty acid β-oxidation supports oxidative phosphorylation and proliferation in cancer cells. Int J Biochem Cell Biol 2015; 65:209–21.
2. Metallo CM, Gameiro PA, Bell EL, Mattaini KR, Yang J, Hiller K, et al. Reductive glutamine metabolism by IDH1 mediates lipogenesis under hypoxia. Nature 2011;481:380–4.
3. Mycielska ME, Milenkovic VM, Wetzel CH, Rümmele P, Geissler EK. Extracellular citrate in health and disease. Curr Mol Med 2015;15:884–91.
4. Mycielska ME, Djamgoz MB. Citrate transport in the human prostate epithelial PNT2-C2 cell line: electrophysiological analyses. J Physiol 2004 559:821–33.
5. Mycielska ME, Palmer CP, Brackenbury WJ, Djamgoz MB. Expression of Na+-dependent citrate transport in a strongly metastatic human prostate cancer PC-3M cell line: regulation by voltage-gated Na+ channel activity. J Physiol 2005;563:393–408.
6. Mazurek MP, Prasad PD, Gopal E, Fraser SP, Bolt L, Rizaner R, et al. Molecular origin of plasma membrane citrate transporter in human prostate epithelial cells. EMBO Rep 2010;11:431–7.

Downloaded from http://aacrjournals.org/cancerres/article-pdf/78/10/2513/2764970/2513.pdf by guest on 13 September 2024

7. Schmidt KM, Hellerbrand C, Ruemmele P, Michalski CW, Kong B, Kroemer A, et al. Inhibition of mTORC2 component RICTOR impairs tumor growth in pancreatic cancer models. Oncotarget 2017;8:24491–505.
8. Schmidt K, Moser C, Hellerbrand C, Zieker D, Wagner C, Redekopf J, et al. Targeting fibroblast growth factor receptor (FGFR) with BGJ398 in a gastric cancer model. Anticancer Res 2015:35:6655–65.
9. Van der Goot AT, Zhu W, Vázquez-Manrique RP, Seinstra RI, Dettmer K, Michels H, et al. Delaying aging and the aging-associated decline in protein homeostasis by inhibition of tryptophan degradation. Proc Natl Acad Sci U S A 2012;109:14912–7.
10. Millard P, Letisse F, Sokol S, Portais J. IsoCor. Correcting MS data in isotope labeling experiments. Bioinformatics 2012;28:1294–6.
11. Dettmer K, Vogl FC, Ritter AP, Zhu W, Nürnberger N, Kreutz M, et al. Distinct metabolic differences between various human cancer and primary cells. Electrophoresis 2013;19:2836–47.
12. Walters DE, Kaplan RS. Homology-modeled structure of the yeast mitochondrial citrate transport protein. Biophys J 2004;87;907–11.
13. Sali A, Blundell TL. Comparative protein modelling by satisfaction of spatial restraints. J Mol Biol 1993;234;779–815.
14. Trott O, Olson AJ. AutoDock Vina: improving the speed and accuracy of docking with a new scoring function, efficient optimization, and multithreading. J Comput Chem 2010;31:455–61.
15. Morris GM, Huey R, Lindstrom W, Sanner MF, Belew RK, Goodsell DS, et al. AutoDock4 and AutoDockTools4: automated docking with selective receptor flexibility. J Comput Chem 2009;30:2785–891.
16. Duan Y, Wu C, Chowdhury S, Lee MC, Xiong G, Zhang W, et al. A point-charge force field for molecular mechanics simulations of proteins based on condensed-phase quantum mechanical calculations. J Comput Chem 2003;24:1999–2012.
17. Lantow M, Viergutz T, Weiss DG., Simkó M. Comparative study of cell cycle kinetics and induction of apoptosis or necrosis after exposure of human Mono Mac 6 cells to radiofrequency radiation. Radiat Res 2006;166: 539–43.
18. Zukunft S, Sorgenfrei M, Prehn C, Möller G, Adamski J. Targeted metabolomics of dried blood spot extracts. Chromatographia 2013; 76:1295–05.
19. Römisch-Margl W, Prehn C, Bogumil R, Röhring C, Suhre K, Adamski J. Procedure for tissue sample preparation and metabolite extraction for high-throughput targeted metabolomics. Metabolomics 2012;8: 133–42.
20. Thevenot EA, Roux A, Xu Y, Ezan E, Junot C. Analysis of the human adult urinary metabolome variations with age, body mass index and gender by implementing a comprehensive workflow for univariate and OPLS statistical analyses. J Proteome Res 2015;14:3322–35.
21. Currie E, Schulze A, Zechner R, Walther TC, Farese RV Jr. Cellular fatty acid metabolism and cancer. Cell Metab 2013;18:153–61.
22. Morad SA, Cabot MC. Ceramide-orchestrated signalling in cancer cells. Nat Rev Cancer 2013;13:51–65.
23. Yang Y, Bedford MT. Protein arginine methyltransferases and cancer. Nat Rev Cancer 2013;13:37–50.
24. Krall AS, Xu S, Graeber TG, Braas D, Christofk HR. Asparagine promotes cancer cell proliferation through use as an amino acid exchange factor. Nat Commun 2016;7:11457.
25. Costello LC, Franklin RB. The clinical relevance of the metabolism of prostate cancer; zinc and tumor suppression: connecting the dots. Mol Cancer 2006;15:5–17.
26. Evans AJ. Alpha-methylacyl CoA racemase (P504S): overview and potential uses in diagnostic pathology as applied to prostate needle biopsies. J Clin Pathol 2003;56:892–7.
27. James EL, Michalek RD, Pitiyage GN, de Castro AM, Vignola KS, Jones J, et al. Senescent human fibroblasts show increased glycolysis and redox homeostasis with extracellular metabolomes that overlap with those of irreparable DNA damage, aging, and disease. J Proteome Res 2015; 14:1854–71.
28. Brar SS, Grigg C, Wilson KS, Holder WD Jr, Dreau D, Austin C, et al. Disulfiram inhibits activating transcription factor/cyclic AMP-responsive element binding protein and human melanoma growth in a metal-dependent manner in vitro, in mice and in a patient with metastatic disease. Mol Cancer Ther 2004;3:1049–60.
29. Schweizer MT, Lin J, Blackford A, Bardia A, King S, Armstrong AJ, et al. Pharmacodynamic study of disulfiram in men with non-metastatic recurrent prostate cancer. Prostate Cancer Prostatic Dis 2013;16:357–61.

Downloaded from http://aacrjournals.org/cancerres/article-pdf/78/10/2513/2764970/2513.pdf by guest on 13 September 2024